

Direct fast heating efficiency of a counter-imploded core plasma employing a laser for fast ignition experiments (LFEX)

journal or publication title	Nuclear Fusion
volume	62
number	9
page range	096013
year	2022-08-05
NAIS	13559
URL	http://hdl.handle.net/10655/00013463

doi: <https://doi.org/10.1088/1741-4326/ac7966>



PAPER • OPEN ACCESS

Direct fast heating efficiency of a counter-imploded core plasma employing a laser for fast ignition experiments (LFEX)






To cite this article: Yoneyoshi Kitagawa *et al* 2022 *Nucl. Fusion* **62** 096013

View the [article online](#) for updates and enhancements.

You may also like

- [Overview of physics studies on ASDEX Upgrade](#)
H. Meyer, for the AUG Team: D. Aguiam, C. Angioni et al.
- [Developing the science and technology for the Material Plasma Exposure eXperiment](#)
J. Rapp, T.M. Biewer, T.S. Bigelow et al.
- [Alpha heating, isotopic mass, and fast ion effects in deuterium–tritium experiments](#)
R.V. Budny and JET Contributors

Direct fast heating efficiency of a counter-imploded core plasma employing a laser for fast ignition experiments (LFEX)

Yoneyoshi Kitagawa^{1,*}, Yoshitaka Mori¹, Katsuhiko Ishii¹, Ryohei Hanayama¹, Shinichiro Okihara¹, Yasunobu Arikawa², Yuki Abe², Eisuke Miura³, Tetsuo Ozaki⁴, Osamu Komeda⁵, Hiroyuki Suto⁵, Yusuke Umetani⁵, Atsushi Sunahra⁶, Tomoyuki Johzaki⁷, Hitoshi Sakagami⁴, Akifumi Iwamoto⁴, Yasuhiko Sentoku², Nozomi Nakajima², Shohei Sakata², Kazuki Matsuo², Reza S. Mirfayzi², Junji Kawanaka², Shinsuke Fujiokua², Koji Tsubakimoto², Keisuke Shigemori², Kohei Yamanoi², Akifumi Yogo², Ayami Nakao², Masatada Asano², Hiroyuki Shiraga², Tomoyoshi Motohiro⁸, Tatsumi Hioki⁸ and Hirozumi Azuma⁹

¹ The Graduate School for the Creation of New Photonics Industries, Kurematsucho 1995-1, Nishiku, Hamamatsu, 431-1202, Japan

² Osaka Univ., ILE, 2-6 Yamada-oka, Suita, 565-0871, Japan

³ AIST, Tsukuba, 305-8560, Japan

⁴ NIFS, 322-6 Oroshi, Toki, 509-5292, Japan

⁵ Advanced Material Engineering Division, Toyota Motor Corporation, Mishuku 1200, Susono 410-1193, Japan

⁶ Purdue Univ., CMUXE, 610 Purdue Mall, West Lafayette, IN 47907, United States of America

⁷ Hiroshima Univ. Eng., 1-4-1 Kagamiyama, Higashi-Hiroshimas, 739-8527, Japan

⁸ Institute of Materials Innovation, Nagoya Univ., Furo-cho, Chikusa-ku, Nagoya 464-8603, Japan

⁹ Aichi SRC, 250-3 Minami-yamaguchi-cho, Seto, 489-0965, Japan

E-mail: kitagawa@gpi.ac.jp

Received 7 April 2022

Accepted for publication 16 June 2022

Published 5 August 2022



CrossMark

Abstract

Fast heating efficiency when a pre-imploded core is directly heated with an ultraintense laser (heating laser) was investigated. ‘Direct heating’ means that a heating laser hits a pre-imploded core without applying either a laser guiding cone or an external field. The efficiency, η , is defined as the increase in the internal core energy divided by the energy of the heating laser. Six beams (output of 1.6 kJ) from the GEKKO XII (GXII) green laser system at the Institute of Laser Engineering (ILE), Osaka University were applied to implode a spherical deuterated polystyrene (CD) shell target to form a dense core. The DD-reacted protons and the core x-ray emissions showed a core density of $2.8 \pm 0.7 \text{ g cm}^{-3}$, or 2.6 times the solid density. Furthermore, DD-reacted thermal neutrons were utilized to estimate the core temperature between 600 and 750 eV. Thereafter, the core was directly heated by a laser for fast-ignition experiments (LFEX, an extremely energetic ultrashort pulse laser) at ILE with its axis lying

* Author to whom any correspondence should be addressed.



Original content from this work may be used under the terms of the [Creative Commons Attribution 4.0 licence](https://creativecommons.org/licenses/by/4.0/). Any further distribution of this work must maintain attribution to the author(s) and the title of the work, journal citation and DOI.

along or perpendicular to the GXII bundle axis, respectively. The former and latter laser configurations were termed ‘axial’ and ‘transverse modes’, respectively. The η was estimated from three independent methods: (1) the core x-ray emission, (2) the thermal neutron yield, and (3) the runaway hot electron spectra. For the axial mode, $0.8\% < \eta < 2.1\%$ at low power (low LFEX energy) and $0.4\% < \eta < 2.5\%$ at high power (high LFEX energy). For the transverse mode, $2.6\% < \eta < 7\%$ at low power and $1.5\% < \eta < 7.7\%$ at high power. Their efficiencies were compared with that in the uniform implosion mode using 12 GXII beams, $6\% < \eta < 12\%$, which appeared near to the η for the transverse mode, except that the error bar is very large.

Keywords: counter implosion, fast ignition, direct heating, heating efficiency

(Some figures may appear in colour only in the online journal)

1. Introduction

The National Ignition Facility, where α burning recently occurred, is a promising candidate for developing a safe fusion power plant [1, 2]. Nevertheless, successful core ignition (breakeven) has not been achieved [3]. A self-ignition scheme, which involves burning the core via imploding, has been unexpectedly challenging. Tabak *et al* had proposed that a fast-ignition scheme may exhibit a complementary ability to ignite the fuel [4].

In the fast-ignition scheme, a pre-imploded DD or DT capsule is irradiated with a laser pulse for a few tens of picoseconds (a much shorter timeframe than that required for the hydrodynamic disassembly of a compressed core). This short-pulse laser generates energetic electrons and ions near the cut-off region. These electrons and ions can penetrate the core and form a hot spot, from which a ${}^3\text{He}$ (an α particle) burning wave spreads over the core. Fast heating and ignition will greatly contribute to energy production from the inertial confinement fusion if they trigger core ignition with high gain.

The scheme of self-ignition fusion must concentrate centripetal shock waves to ignite a central hot spark [5]. Nevertheless, this requires fully symmetric 4π laser-beam illumination. For future fusion plants, fully symmetric laser illumination will be unrealistically difficult to construct and operate. By contrast, the fast-ignition scheme does not require fully symmetric implosion since the fast-ignition laser can generate a hot spark in any core area.

Although the concept of a fast ignition scheme is attractive, so far neither a hot spark has been formed in a compressed core, nor has efficient core heating been observed. The present study is aimed at clearly indicating whether or not fast ignition can boost ignition, even if the core is not symmetrically imploded. The study also aims to get a scaling law of the fast-ignition efficiency. As a first step, we are to evaluate a value of η in the nonuniform implosion.

Six beams (output of 1.6 kJ) from the GEKKO XII (GXII) green laser system at the Institute of Laser Engineering (ILE), Osaka University were applied to implode a spherical deuterated polystyrene (CD) shell target to form a dense core. Thereafter, the core was directly heated by a laser for fast ignition experiments (LFEX, an extremely energetic ultrashort pulse

laser) at ILE with its axis lying along or perpendicular to the GXII bundle axis, respectively. Here ‘direct heating’ means that a heating laser hits a pre-imploded core without applying any laser guiding cone or any external field.

We first applied the petawatt module laser (90 J output/0.8 ps) as a heating laser to demonstrate the feasibility of direct core heating (2001) [6]. This laser enhanced the yield of DD-reacted thermal neutrons by a factor of 1.7; the yield (Y_n) was enhanced from $4 \times 10^5/4\pi$ sr to $7 \times 10^5/4\pi$ sr. The subsequent petawatt laser (PWL, 190 J output/0.7 ps) exhibited the enhancement of Y_n with a factor of 4.1 ± 3.6 , i.e., from $(1.0 \pm 0.6) \times 10^6/4\pi$ sr to $(4.1 \pm 1.2) \times 10^6/4\pi$ sr [7–9].

Thus far, a core plasma with a density as low as ~ 10 g cm $^{-3}$ and a temperature as low as ~ 1 keV has demonstrated the feasibility of fast heating, but the core heating efficiency has yet to be estimated. It is necessary to construct a scaling law of the efficiency valid for a high gain target.

For a step towards this, we compare here the heating efficiency of two illumination configurations, (figures 1(a) and (b)). The first mode (figure 1(a)) is the simplest, although its cutoff point is far from the core and many plasma clouds block the transport of hot electrons and ions [8]. The second mode (figure 1(b)), which exhibits the same configuration as reported in [10, 11], may not be as simple. Nonetheless, its cutoff point is closer to the core, and so less cloud plasma reduces transport blocking [10, 11]. A comparison of these modes will result in the best configuration for asymmetrical illumination and also determine the effect of the cloud plasma on the transportation of energetic particles to the core.

2. Experimental setup and the core plasma

2.1. Target and lasers

The target was set at the center of a vacuum chamber, made of SUS314. The chamber is 1.6 m in diameter with 8 cm-thick walls. Counter-propagating beams from the GXII laser (the wavelength is $0.527 \mu\text{m}$) exhibiting a third-order super-Gaussian pulse shape (pulse width = 1.3 ns) were applied to implode the CD spherical shell target. We used two types of targets, a simple shell and a shell with two $200 \mu\text{m}$ -diameter holes, as shown in the top corners of figures 1(a) and (b),

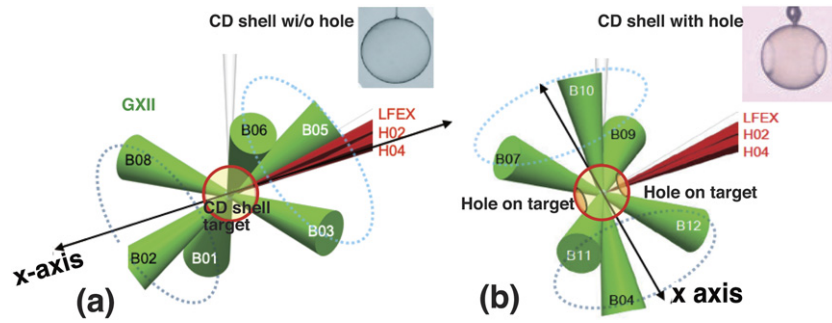


Figure 1. Schematic illustrating six imploding beams, GXII (green), and one heating beam, LFEX (red): (a) axial mode, where three GXII beams approach from the left and the other three from the right side. LFEX lies along the x -axis (the bundle axis). Each GXII beam (F/3) was 37° along the x -axis and tangentially focused on the target. The dotted circles show a group of the three adjacent B01, B02, and B08 beams and the other group of B03, B05, and B06 ones. The right top image is the shell target with no hole. (b) Transverse mode, where the LFEX lies perpendicular along the x -axis (the bundle axis). Three adjacent GXII beams (B07, B09, and B10 or B04, B11 and B12) converge to the center at an angle of 11° . The bundle axis is along the x -axis and the right top image is the shell target with two holes.

respectively. The diameter and thickness of the shell were 501 ± 10 and $6.9 \pm 0.6 \mu\text{m}$, respectively. For the transverse mode, we utilized a target with two holes as shown in figure 1(b) right top: one was a window for LFEX, and the other for the x-ray detectors [10, 11]. The holes kept both LFEX and x-ray emissions from hitting the non-ablated solid shell.

The ratio of the focal distance (d) to the shell radius (R), d/R , was -3 . d is the distance from the target center to the focal point, and the negative sign means downstream along the laser propagation direction. Each GXII beam (F/3) was bundled at 37° along the x -axis and was tangentially focused on the target. The spot size of each beam on the target was $500 \mu\text{m}$ and the total output energy was $1.64 \text{ kJ} \pm 0.63 \text{ kJ}$. The pointing of GXII was $50 \mu\text{m}$. Energy imbalance between the six beams was 6.7% and 9.6% for axial and transverse modes, respectively.

The wavelength and pulse width of LFEX laser were $1.05 \mu\text{m}$ and 1.5 ps pulse, respectively. The laser was directly focused on the center of the core (F/10). The focal spot was $60 \mu\text{m}$ in diameter and the on-target energy of 300 J gives an intensity of $7 \times 10^{18} \text{ W cm}^{-2}$. The pointing accuracy of LFEX was less than $50 \mu\text{m}$. At the front end LFEX has an OPCPA, which makes the single mode pulse and is reflected by a deformable mirror before is focused on target. The smoothness of beam cross sections of GXII and LFEX are in figures 2(a) and (b).

For the first experiment, the total output energy of the GXII was $1.64 \text{ kJ} \pm 0.63 \text{ kJ}$ and that of the LFEX energy was between 250 J and 350 J . For the second experiment, the GXII total output energy was reduced to $1.35 \text{ kJ} \pm 0.09 \text{ kJ}$, whereas that of the LFEX was increased to $840 \text{ J} \pm 50 \text{ J}$. We termed the former experiment as low power mode and the latter as high power mode, respectively.

2.2. STAR-2D-ALE simulation of the counter implosion

The two-dimensional hydrocode ‘STAR 2D arbitrary Lagrangean–Eulerian code (STAR-2D-ALE)’ was developed to simulate axial and transverse implosions by counter beams propagated from GXII [12]. Figure 3(a) shows the x-ray emission for the axial mode at 2.83 ns , which was the maximum

compression timing, $+330 \text{ ps}$ after the GXII peak resulting in an electron temperature (T_e) of $\sim 800 \text{ eV}$, mass density (ρ) of $\sim 2 \text{ g cm}^{-3}$ and a thermal DD neutron yield (Yn) equal to $2.63 \times 10^5/4\pi \text{ sr}$. The shell is mainly compressed in the x direction and the core looks like a pancake.

Figure 3(b) shows the maximum compression for the transverse mode, $+360 \text{ ps}$ after the GXII peak. In this case the shell is mainly compressed in the y direction, and the core resembles a sausage. The difference in the timing in figures 3(a) and (b) was due to the difference in their laser configurations, as described in [12]. The simulation postulates for the transverse mode that $T_e \sim 600 \text{ eV}$, $\rho \sim 3 \text{ g cm}^{-3}$, and $Yn = 4.2 \times 10^5/4\pi \text{ sr}$.

2.3. X-ray emission from the imploded core

We positioned two x-ray pinhole cameras at 55° and 109° relative to the LFEX incidence (x -axis). The detection window of the camera was ranged from roughly 10 keV to 50 keV . We constructed the core shape using simultaneous emission images from these two directions.

Figure 4(a) exhibits an ellipse for the axial mode, whose major axis lies in the z -axis. This ellipse looks like the simulation for the axial mode shown in figure 3(a). Supposing the axial symmetry, we estimated the radii in the x , y , and z directions, R_x , R_y , and R_z to be $37.7 \mu\text{m} \pm 1.9 \mu\text{m}$, $37 \mu\text{m} \pm 1.8 \mu\text{m}$, and $56 \mu\text{m} \pm 2.8 \mu\text{m}$, respectively. The volume, V_A , is estimated as $(3.2 \pm 0.5) \times 10^{-7} \text{ cm}^3$.

Regarding the transverse mode, figure 4(b) shows an ellipse whose major axis lies in the x -axis. This looks like the simulation of figure 3(b). $R_x = 81.1 \pm 4 \mu\text{m}$, $R_y = 40.6 \pm 2 \mu\text{m}$ and $R_z = 32 \pm 1.6 \mu\text{m}$. The volume V_T is estimated as $(4.4 \pm 0.7) \times 10^{-7} \text{ cm}^3$.

Considering the pointing accuracy of LFEX of less than $50 \mu\text{m}$, a spot area of LFEX on the focal point is within $9.5 \times 10^{-5} \text{ cm}^2$. Both the core area of $6.5 \times 10^{-5} \text{ cm}^2$ in the axial mode and of $4.0 \times 10^{-5} \text{ cm}^2$ in the axial mode are near to the LFEX spot area. Hence, LFEX could illuminate the core both in the axial and transverse modes.

Figure 4(c) shows that the peak of the GXII laser is at 1.79 ns and the x-ray emission peak is at 2.0 ns . The delay

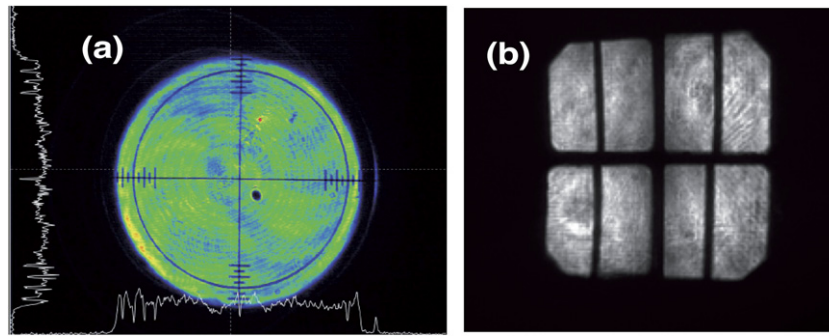


Figure 2. (a) GXII B05 beam (beam diameter is 312 mm). (b) Four-segmented LFEX beam (cross section is 80 cm \times 80 cm).

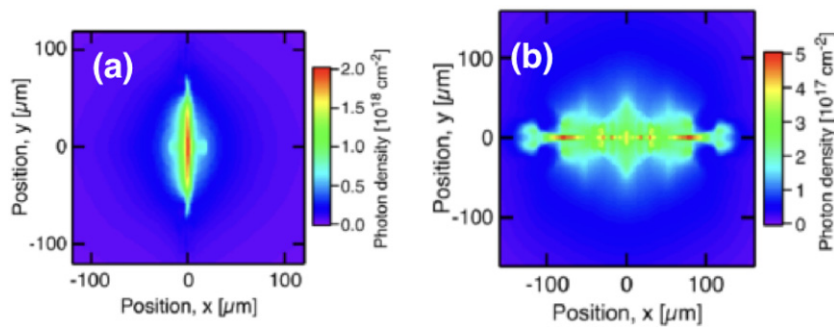


Figure 3. STAR 2D arbitrary Lagrangian–Eulerian simulation of GXII counter-implosion shows, applying a postprocessor for ray tracing and a fine structure of self-emitted x-ray for (a) the axial mode at 2.83 ns (delay between maximum compression and rise time of GXII with a simple CD shell target) and (b) transverse mode at 2.86 ns (the delay of the maximum compression time from the rise time of GXII) with a target having two 200 μm holes. The GXII peak was at 2.50 ns [12].

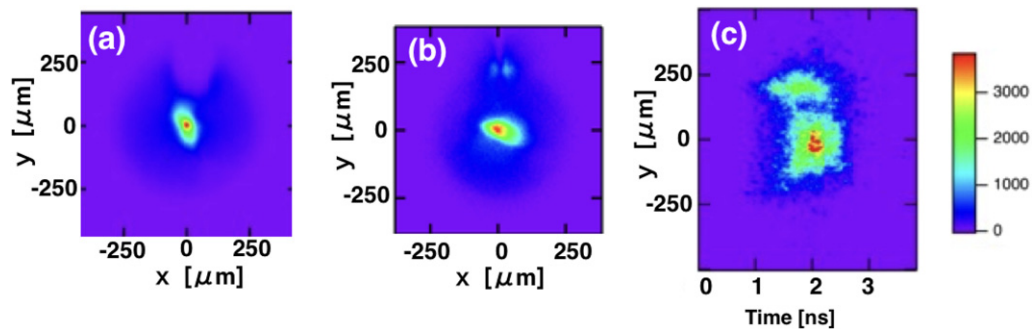


Figure 4. Pinhole images of x-ray emission from the core. (a) Image from the camera set at 55° for the axial mode without LFEX (#24T1) with GXII at 1.619 kJ. Three GXII beams propagate from the left direction, lying along the x -axis. The other three beams were from the right direction. (b) Image from the camera set at 109° for the transverse mode without LFEX (#25T1) with GXII at 1.553 kJ. Each beam propagates from the upper and lower directions, perpendicular to the x -axis. The detection window is 4 keV–50 keV. (c) X-ray streak photograph of the same shot as (a). The GXII peak was 1.79 ns after the time origin of the streak camera. The upper emission observed in the streak image (y approximately $+250 \mu\text{m}$), came from the target stalk. The detection window is 1.5–10 keV. The temporal resolution of the streak camera was 40 ps, but its shot-by-shot jitter was 100 ps [12]. # is the shot number.

between GXII and x-ray peaks was $+290 \pm 40$ ps, which is close to the simulated maximum compression delay of $+330$ ps from the GXII peak (figure 3(a)).

2.4. ρR and ρ of the imploded core plasma for the axial mode

The DD ($d(d, n)^3\text{He}$) reaction produced 3.02 MeV protons. We assumed the reaction at the center of the core and a downward

shift of proton energy on its way through the core. The shift is proportional to the areal density (ρR) of the path of proton flight. We set two CR-39 proton track detectors: one along the z -axis (90° from LFEX) and the other 21° from LFEX (nearly along the x -axis) for the axial mode. The detectors were positioned 5 cm away from the target and the size of CR-39 film was a 0.4 mm \times 0.6 mm square. The x -direction detector measured ρR along the x -axis and the z -direction one obtained ρR along the z -axis [13, 14]. The striped columns in figure 5

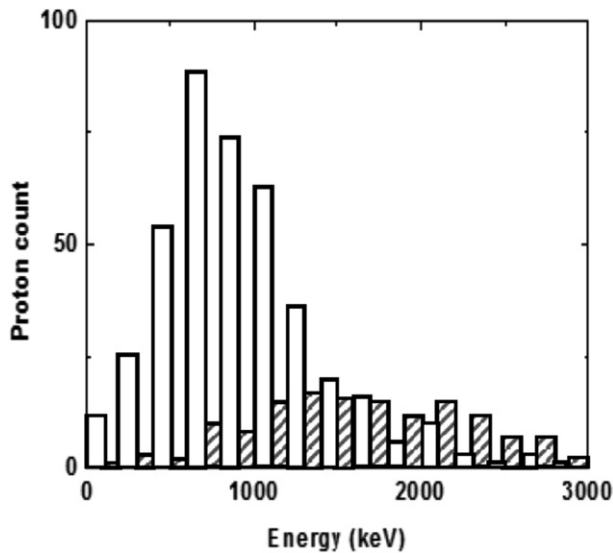


Figure 5. Energy spectra of DD-reacted protons without LFEX, obtained using two CR-39 track detectors 90° and 21° from LFEX. The DD reaction was composed of two branches: one yields neutrons (2.45 MeV) and the other, which was utilized here, yields protons (3.02 MeV). The white columns present the spectrum that was shifted from 3.02 MeV along the z -axis (perpendicular to LFEX). The striped columns are the count 21° from LFEX (x -axis) [13, 14].

show that the energy peak shifts to $1.50 \text{ MeV} \pm 0.5 \text{ MeV}$, which yielded a ρR of $(0.011 \pm 0.003) \text{ g cm}^{-2}$ along the x -axis. The white columns show the peak shift from 3.02 MeV to $0.75 \text{ MeV} \pm 0.25 \text{ MeV}$, which yielded a ρR of $(0.016 \pm 0.002) \text{ g cm}^{-2}$ along the z -axis.

Applying $R_x = 37.7 \mu\text{m} \pm 1.8 \mu\text{m}$ from figure 4(a) and $\rho R = (0.011 \pm 0.003) \text{ g cm}^{-2}$ from figure 5, we obtained $\rho = (2.9 \pm 0.9) \text{ g cm}^{-3}$ along x axis. Applying $R_z = 56 \mu\text{m} \pm 2.8 \mu\text{m}$ and $(0.016 \pm 0.002) \text{ g cm}^{-2}$ yielded $(2.85 \pm 0.49) \text{ g cm}^{-3}$ along the z axis. The CD core comprises deuteron and carbon ions.

The value of ρ , averaged over the x and z -axes, is $(2.87 \pm 0.7) \text{ g cm}^{-3}$, i.e., 2.6 times the solid density. Then, the averaged ion number density, n_i , is $(2.45 \pm 0.6) \times 10^{23}/\text{cm}^3$. Since the core temperature was sufficiently high to facilitate full ionization, Z_{CD} was 3.5, resulting in the electron number density $n_e = Z_{\text{CD}}n_i = (8.57 \pm 2.0) \times 10^{23}/\text{cm}^3$.

2.5. T_0 of the imploded core plasma for the axial mode

Without hitting the LFEX, the neutron scintillator array ‘MANDALA’ measured the 2.45 MeV yield Yn to be $(3.47 \pm 0.18) \times 10^6/4\pi \text{ sr}$, as shown later in figure 8(a) [15, 16]. A clear thermal neutron peak at 2.45 MeV appears to show that the imploded core was almost thermalized. Yn is given by $(n_i/4)^2 \langle \sigma v \rangle_T V \tau$, from which we can estimate the core temperature, T . Here $\langle \sigma v \rangle_T$ indicates the thermal fusion-reactivity, i.e., a fusion cross-section-velocity product averaged over the Maxwell distribution. τ is the burning time (a minimum of the stagnation duration).

Using the obtained n_i , V_A , and Yn values, we estimated T_0 to be $0.75 \text{ keV} \pm 0.1 \text{ keV}$. Since for $0.6 \text{ keV} \leq T_0 \leq 0.8 \text{ keV}$, $\langle \sigma v \rangle_T$ can be approximated by a line proportional

to $T^{6.0 \pm 0.8}$; we supposed $T \propto Yn^{1/(6 \pm 0.8)}$. τ can be expressed as $R/4C_s$ (C_s is a sound velocity $\sim 2.4 \times 10^7 \text{ cm s}^{-1}$), which was $44 \text{ ps} \pm 2 \text{ ps}$ at $T_0 = 0.7 \text{ keV}$. Thereby, we estimated the internal energy of the core, $E_{\text{int}} = 3/2n_i(Z_{\text{CD}} + 1)T_0V$, to be $63 \text{ J} \pm 25 \text{ J}$. Hence, the estimated T_0 is somewhat lower than the ion temperature of $T_0 \leq 0.8\text{--}1.0 \text{ keV}$ from spectrum broadening (figure 8(a)).

2.6. ρ and T_0 of the imploded core plasma for the transverse mode

We have not directly measured the core density for the transverse mode. However, since STAR-2D-ALE predicted this value to be within 2 g cm^{-3} and 3 g cm^{-3} , we assumed the density is the same for both axial and transverse modes. In section 4.2, we will estimate T_0 to be $0.6 \text{ keV} \pm 0.05 \text{ keV}$ and E_{int} to be $65 \text{ J} \pm 39 \text{ J}$ for the transverse mode.

3. Axial mode heating

3.1. X-ray emission for the axial mode

The streak camera image of figure 6(a) shows that LFEX heats the core when the LFEX timing is set at 2.0 ns (+200 ps after the GXII pulse peak at 1.8 ns). However, when LFEX is at 2.4 ns as in figure 6(b), the emission exhibited no apparent feature at 2.0 ns, but a small heating feature at 2.4 ns. The intensity of the emission peak in figure 6(a) is equal to or more than 1.3 times larger than that in figure 6(b).

X-ray pinhole images in figures 7(a)–(c) show that the emission was the strongest at figure 7(b) +200 ps. Figure 7(d) shows that red (#4T1) was 1.43 ± 0.09 times stronger than either blue (#4T2) or green (#4T4) and was 1.11 ± 0.15 times stronger than that of the dashed (#5T3) without LFEX hitting. Considering ≥ 1.3 times in figure 6(a) and 1.11 ± 0.15 times in figure 7(b), LFEX seems to enhance the intensity by 1.27 ± 0.15 times. The focal spot of LFEX is $60 \mu\text{m}$ in diameter. Figure 7(d) shows that the core emission area is the same as that before LFEX hits (dashed line), which is $2R_y \times 2R_z = (74 \pm 3.6) \mu\text{m} \times (112 \pm 5.6) \mu\text{m}$, as in section 2.3. It was $2R_y \times 2R_z = (81 \pm 8) \mu\text{m} \times (64 \pm 6) \mu\text{m}$ in the transverse mode.

Figure 7(e) plots the mean free paths of the Rosseland and Plank absorptions, respectively. To estimate the radiant energy in the perfect equilibrium state, we can use the Planck spectral radiant energy density, which is given as $U_{\nu p} = 8\pi h\nu^3/c^3(e^{h\nu/k_B T} - 1)$. This leads us to the Planck absorption mean free path, which is given by $l_p = 1.6 \times 10^{23} T^{0.7/2}/Z^2 N_+ N_e$ (cm). When the core size is longer than l_p , we can say that the core radiation is in the equilibrium state.

Conversely, in a nonequilibrium state, the radiation mean free path becomes the Rosseland mean free path, which is given by $l_R = 4.86 \times 10^{24} T^{0.7/2}/Z^2 N_+ N_e$ (cm) and is now one order longer than l_p [17].

Both the l_p and l_R are plotted as a function of T in figure 7(e). The vertical axis is not a length l , but a ρl [18]. The experimental point of ρR is between the two curves, i.e., the core

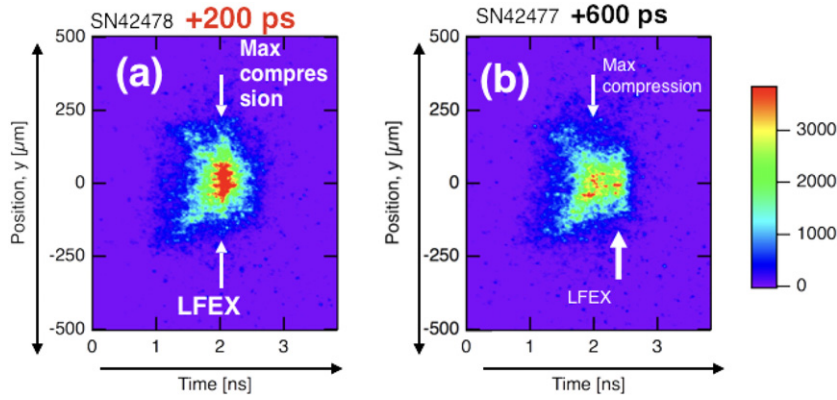


Figure 6. X-ray streak camera images of the heated core at low power: (a) LFEX at 2.0 ns (+200 ps after the GXII pulse peak #24T3) and (b) at 2.4 ns (+600 ps after GXII peak #24T2) GXII pulse peak is at 1.79 ns. The timing jitter was 100 ps.

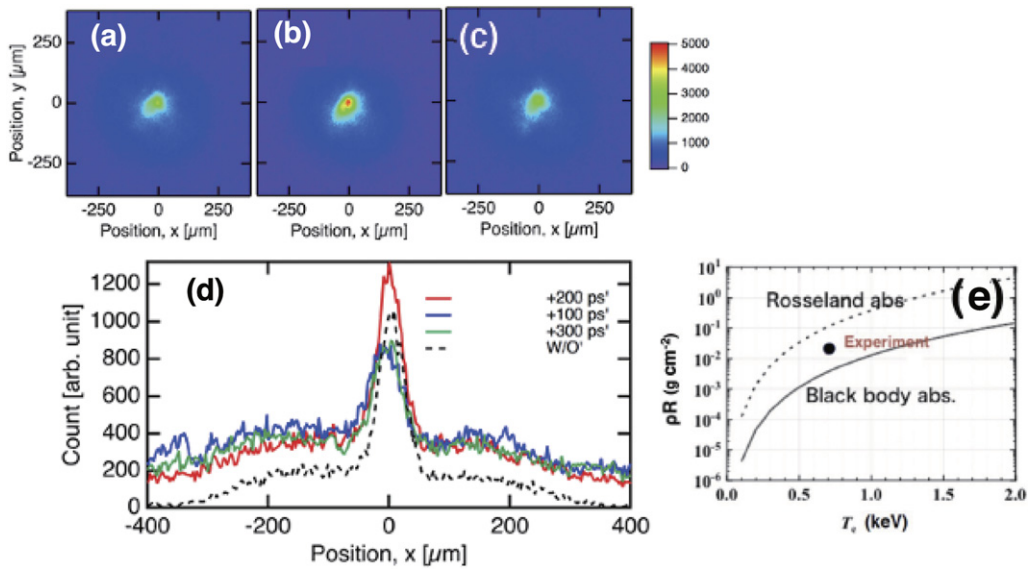


Figure 7. X-ray pinhole images at high power: (a) LFEX of 890 J at +100 ps, GXII of 1.34 kJ (#4T2); (b) LFEX of 779 J at +200 ps, GXII of 1.42 kJ (#4T1); (c) LFEX of 898 J at +300 ps, GXII of 1.31 kJ (#4T4); and (d) x-axis-scanned emissions corresponding to (a) blue (#4T2), (b) red (#4T1), and (c) green (#4T4), and dashed (#5T3) [12]. (e) Rosseland and Planck absorption mean-free-paths as functions of T_e . The solid point was from the experiment (expressed by ρR) [17, 18].

radius is longer than l_p , but shorter than ρ_R , which may permit us to approximate the core radiation in the equilibrium state.

Since the detection window is roughly between 4 keV and 50 keV and the emission peak will be around 2 keV, we probably observe the high frequency region, where $x = h\nu/kT \gg 1$. Supposed the emission is a Planckian, the detected radiant energy from ν_0 to ν is given by [17]

$$\begin{aligned}
 U_p &= \int_{\nu_0}^{\nu} U_{\nu p} d\nu = \int_{\nu_0}^{\nu} \frac{8\pi h\nu^3}{c^3} \frac{d\nu}{e^{h\nu/k_B T} - 1} \\
 &= \frac{8\pi(k_B T)^4}{c^3 h^3} \int_{x_0}^x \frac{x^3 dx}{e^x - 1}.
 \end{aligned} \quad (1)$$

Here (x_0, x) is the spectral region of the detector window. For $x_0 = h\nu_0/kT = 4$ and $x = h\nu/kT = 50$, the numerical

integral $\int_4^{50} x^3/(e^x - 1)dx$ gives 2.61. Hence, $U_p(4, 50) = 8\pi(k_B T)^4/c^3 h^3 \times 2.61$. Any change of the window width does not change T^4 dependence of Planck emission.

Thus, we assumed that the increase in the core temperature is proportional to one fourth the power of the emission ratio, which yields a temperature increase, $\Delta T = ((1.27 \pm 0.15)^{1/4} - 1) T_0 = 45 \pm 27$ eV, and an energy increment, $\Delta E = 3.8 \pm 3.2$ J, using $T_0 = 0.75$ keV ± 0.1 keV and 63 J ± 25 J, respectively from section 2.5. The heating efficiency, $\eta_{x\text{-ray}}$, defined as $\Delta E/\text{LFEX}$ was at high power (779 J #4T1) $(3.8 \pm 3.2)/779 = 0.5\% \pm 0.4\%$. Because of the low temperature increment, $\eta_{x\text{-ray}}$ included a large error bar, which decreased the reliability of the data.

At low power (261 J #24T3), the emission enhancement was 1.4 ± 0.3 times as much as that without LFEX (#24T1), resulting in $\eta_{x\text{-ray}} = 2.1\% \pm 1.8\%$.

3.2. Neutron enhancement for the axial mode

As mentioned in section 2.5 and figure 8(a), the imploded core was almost thermalized to yield a clear thermal neutron peak at 2.45 MeV. T_i in the figure is somewhat higher than that due to Yn , discussed there.

LFEX generated many hot electrons on the path through a peripheral underdense plasma, which drew the energetic protons, deuterons and carbons into the core. Some of the electrons and ions directly heated the core plasma to yield the thermal neutrons [10]. Some of the deuterons collided directly with deuterons in the core or in the periphery of the core to produce neutrons exhibiting a broad spectrum, beam fusion neutrons (figures 8(b) and (c)).

At +600 ps (+400 ps after the maximum compression), beam-fusion neutrons and nonthermal ones were observed (figure 8(c)), but no thermal component was apparent. We could not distinguish an apparent yield enhancement in (b) from (a), but we could compare the spectral temperatures of the 2.45 MeV peaks between (b) and (a). The spectral temperature enhancement $\Delta T = (1.5 \pm 0.6) \text{ keV} - (1.0 \pm 0.2) \text{ keV} = 0.5 \text{ keV} \pm 0.2 \text{ keV}$, and $\Delta T/T_0 = 0.7(1 \pm 0.9)$, leading to $\Delta E = \Delta T/T_0 E_{\text{int}} = 41 \text{ J} \pm 36 \text{ J}$. Thereafter, η_{neutron} might be $(41 \pm 36)/261 = 16\% \pm 13\%$ at low power (#24T3). Since, however, the error bars of the spectral broadening are too large to estimate η_{neutron} , we could not know whether η_{neutron} is meaningful or not, that is to say, the LFEX heated the core or not.

At high power, we could distinguish the thermal component around 2.45 MeV (figure 9(c)) from the broad background signals in figure 9(b). Broad background signals that appear in figure 9(b) are primarily caused by neutrons generated in the materials around the target (the vacuum chamber wall, diagnostics etc) by complex nuclear reactions, including photonuclear and ion-induced reactions ($\text{Fe}(\gamma, n)$, $\text{Fe}(d, n)$, $\text{Al}(p, n)$, $\text{Be}(d, n)$, etc). Neutrons from these complex reactions have an exponentially decaying energy spectrum, resulting in a unique time-of-flight (TOF) distribution that is almost unaffected by laser and target configuration. Thus, we fitted a typical background TOF profile to the experimental results in figure 9(b) and extracted DD-neutron components to figure 9(c). Here, the background fitting was performed in the time domain of 200–800 ns excluding the arrival time of DD neutrons ($t = 600\text{--}650 \text{ ns}$) [16].

$Yn = (1.4 \pm 0.07) \times 10^6/4\pi \text{ sr}$ without LFEX (figure 9(a)) was enhanced to $(8 \pm 0.4) \times 10^6/4\pi \text{ sr}$ (figure 9(c)), that is $(5.7 \pm 0.5) \times Yn$ without LFEX.

The thermal neutron yield, Yn , is given by $Yn = (n_i/4)^2 \langle \sigma v \rangle_T V \tau$. Thereby, MANDALA exhibited T_0 of $0.75 \pm 0.1 \text{ keV}$ and E_{int} of $63 \pm 25 \text{ J}$ without LFEX heating for axial mode.

In so narrow region as $0.6 \leq T \leq 0.8 \text{ keV}$, $\langle \sigma v \rangle_T$ can be approximated by a line proportional to $T^{6.0 \pm 0.8}$, so we supposed $T \propto Yn^{1/(6 \pm 0.8)}$. Thereby, the neutron enhancement of $(5.7 \pm 0.5) \times$ yielded ΔT to be $((5.7 \pm 0.5)^{1/(6 \pm 0.8)} - 1) T_0 = (0.32 \pm 0.06) T_0 = 240 \text{ eV} \pm 70 \text{ eV}$, and $\Delta E = (0.32 \pm 0.06) E_{\text{int}} = 20.1 \text{ J} \pm 11.8 \text{ J}$. Thereafter, $\eta_{\text{neutron}} = (20 \pm 11)/779 = 2.5\% \pm 1.5\%$ at high power (779 J #4T1).

3.3. Hot electrons for the axial mode

We placed three electron spectrometers ‘ESM’ at 0° , 21° , and 70° , respectively, along the x -axis. LFEX was propagated from the 180° direction. ESM distinguished hot runaway electrons from the target. Figure 10(a) shows that the current is the strongest along the 0° direction (x -axis). Figure 10(b) exhibits a slope temperature of $8.7 \text{ MeV} \pm 0.4 \text{ MeV}$ along 0° (#4T1). The stopping range of the electron is given by the equation $\rho R = 0.407E^{1.38} \text{ g cm}^{-2}$ (E in MeV) for $E < 0.8 \text{ MeV}$ [19]. Then, the core plasmas of $\rho R = 0.016 \text{ g cm}^{-2}$ absorb hot electrons $< 0.1 \text{ MeV}$.

Ultraintense laser accelerates hot electrons in the underdense plasmas around the precompressed core [8, 20, 21]. In a previous report, 2D PIC had predicted that 90% of PW laser energy is converted to hot electrons [8]. At the same time, the photon pressure might drive hot electrons at the critical density close to the solid shell. It drives to a few MeV or less electrons, which is much lower than that shown in figure 10 or figure 13.

We have measured the reflection of LFEX from a diamond-like carbon plate. The reflectivity was $\sim 25\%$ at an LFEX of 800 J, as in [22], leading to the upper limit of the hot electron conversion to be 75%. Hence, assuming that 75% of the LFEX energy is converted to the electrons, then the core deposition becomes $0.1/(8.7 \pm 0.4) \times 779 \times 0.75 = 6.7 \text{ J} \pm 0.3 \text{ J}$, for the case of figure 10(b) at an LFEX of 779 J (high power #4T1). The heating efficiency due to hot electrons, η_{electron} , is defined as a deposit of hot electron energy (an increment due to hot electrons) divided by the LFEX energy. Thereafter, η_{electron} is $(6.7 \pm 0.3)/779 = 0.9\% \pm 0.04\%$.

Conversely, Freeman *et al* and Norreys *et al* had reported that the energy conversion from laser to hot electrons is 30% at the critical density of a solid target [23, 24]. If we suppose a conversion of 30%, the heating efficiency is reduced to 0.4 times. In table 1, η_{electron} is written $0.9\% \pm 0.04\%$ at 75% conversion and $0.36\% \pm 0.02\%$ at 30% conversion at high power.

At the low power LFEX of 261 J (#24T3), a slope temperature was $3.98 \text{ MeV} \pm 0.04 \text{ MeV}$, leading to that the energy converted to hot electrons E_{conv} would be $0.1/(3.98 \pm 0.04) \times 261 \times 0.75 = 4.9 \text{ J} \pm 0.05 \text{ J}$ at 75% conversion and $0.1/(3.98 \pm 0.04) \times 261 \times 0.3 = 2.0 \text{ J} \pm 0.02 \text{ J}$ at 30%, respectively. Thereafter, $\eta_{\text{electron}} = E_{\text{conv}}/\text{LFEX}$ will be $1.9\% \pm 0.2\%$ at 75% conversion and $0.8\% \pm 0.08\%$ at 30% conversion (#24T3).

4. Transverse mode heating

4.1. X-ray emissions for the transverse mode

The x-ray emission of the core (figure 11(c)) was two times larger than in figure 11(a), leading to $\Delta T = (2^{1/4} - 1) T_0 = 0.19 T_0 = 114 \text{ eV} \pm 9.5 \text{ eV}$ and ΔE of $12.3 \text{ J} \pm 7.4 \text{ J}$. Figure 11(d) shows that the core emission size (FWHM) when LFEX hits it, is the same as that before LFEX hits (dashed line), as same as in figure 7(d). Hence, the enhancement of the x-ray emission yielded $\eta_{x\text{-ray}} = 1.5\% \pm 0.9\%$ at a high power 832 J.

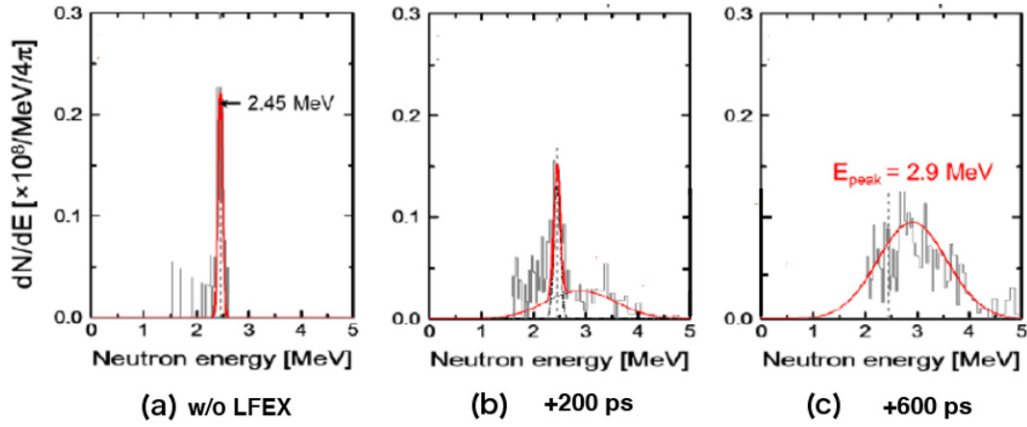


Figure 8. Axial-mode neutron spectra obtained by MANDALA at low power: (a) without LFEX (#25T7), $Y_n = (3.5 \pm 0.59) \times 10^6/4\pi$ sr and $T_i = 1.0 \pm 0.2$ keV for GXII energy of 1.65 kJ, (b) with LFEX of 261 J at +200 ps (#24T3): thermal $Y_n = (2.9 \pm 0.49) \times 10^6/4\pi$ sr and $T_i = 1.5 \pm 0.6$ keV, and beam fusion $Y_n = 6.9 \times 10^6/4\pi$ sr and $T_i = 366$ keV. (c) With LFEX of 336 J at +600 ps (#24T2): beam fusion $Y_n = 1.6 \times 10^7/4\pi$ sr and $T_i = 2.9$ MeV. Red curve is the best fitted one, and T_i is obtained from its broadening.

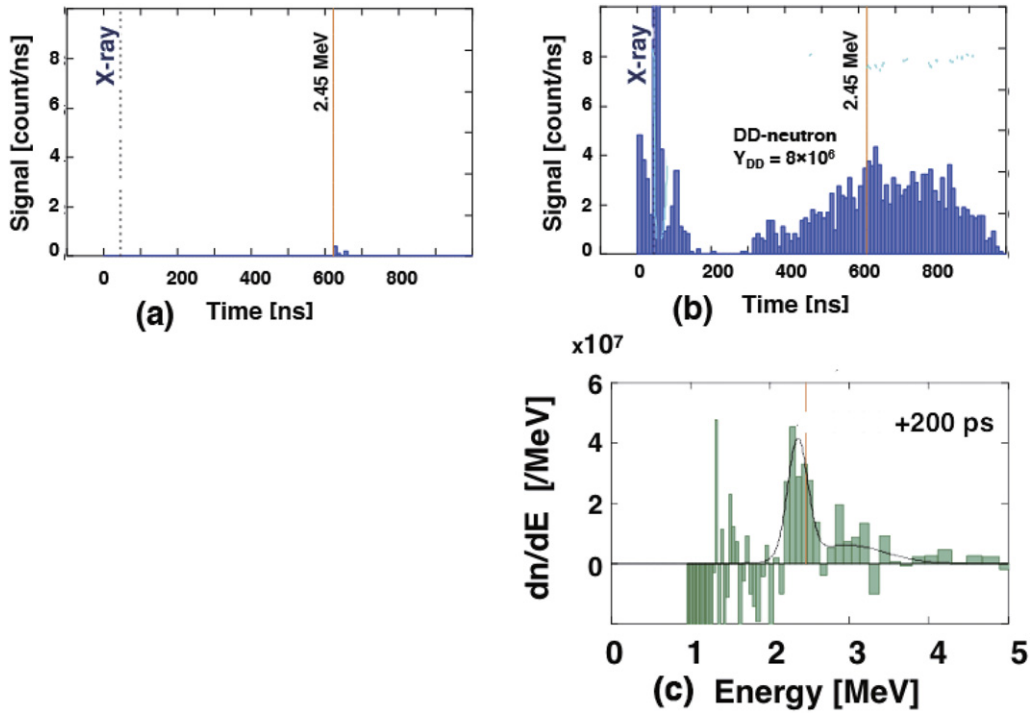


Figure 9. Time-of-flight (TOF) signals of the neutrons at high power for the axial mode: (a) without LFEX (#5T3), $Y_n = (1.4 \pm 0.07) \times 10^6/4\pi$ sr at the GXII energy of 1.38 kJ; (b) GXII of 1.428 kJ with LFEX of 779 J at +200 ps (#4T1 at high power); (c) the same as (b), but the background was subtracted and the resulting TOF was converted to the energy spectrum. $Y_n = (8 \pm 0.4) \times 10^6/4\pi$ sr [15, 16].

At a low power of 342 J (−200 ps (#25T2)), we could not detect the enhancement of the intensity peak but did detect twice the broadening of the emission area, which suggested $\eta_{x\text{-ray}}$ might be 0%–7%.

4.2. Neutron enhancement for the transverse mode

We assumed that the density of the core without LFEX heating is the same as that for the axial mode.

For the transverse mode at high power (figure 12(a)), Y_n without LFEX was $(5.0 \pm 2.0) \times 10^5/4\pi$ sr. Supposing $n_i =$

$(2.45 \pm 0.6) \times 10^{23} \text{ cm}^{-3}$, $V_T = (4.4 \pm 0.7) \times 10^{-7} \text{ cm}^3$ and $\tau_T = 49 \pm 2$ ps, we estimated T_0 to be $600 \text{ eV} \pm 50 \text{ eV}$ and E_{int} to be $65 \text{ J} \pm 39 \text{ J}$. The result shows that LFEX enhanced Y_n from (a) $(5.0 \pm 2.0) \times 10^5/4\pi$ sr to (b) $(3.1 \pm 0.09) \times 10^7/4\pi$ sr, i.e., (62 ± 26) times at the maximum compression, thereby obtaining ΔT of $((62 \pm 26)^{1/(6 \pm 0.8)} - 1) T_0 = (0.98 \pm 0.07) T_0 = 590 \text{ eV} \pm 110 \text{ eV}$, and $\Delta E = (0.98 \pm 0.07) E_{\text{int}} = 64 \text{ J} \pm 46 \text{ J}$. Hence, $\eta_{\text{neutron}} = (64 \pm 46)/832 = 7.7\% \pm 5.5\%$ at high power for the transverse mode.

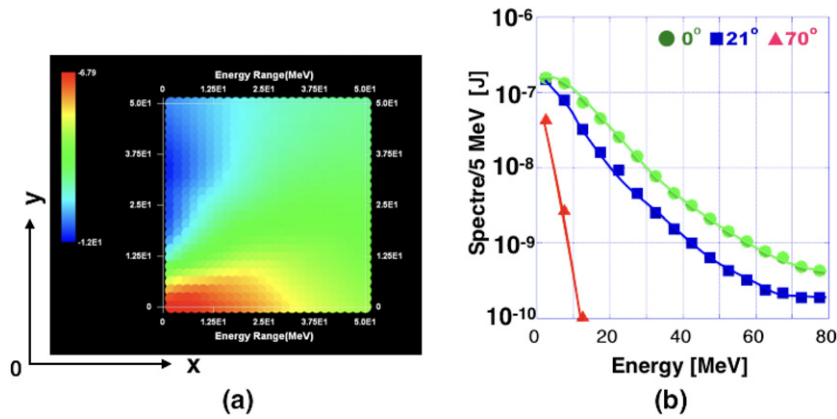


Figure 10. (a) Runaway electron current distribution map for the axial mode (high power #4T4) and (b) its spectrum: the solid circle (green) is 0° , the square (blue) is 21° and the triangle (red) is 70° , respectively, along the x -axis. LFEX of 779 J at +200 ps (high power #4T1) and GXII of 1.44 kJ. ESM was 87.8 cm far from the target (the solid angle 1.0×10^6 sr) and comprised a CR-39 film and a dipole magnet of 0.25 T.

At low power, #25T2, MANDALA detected a single peak of $2.5 \times 10^8/4\pi$ sr at 2.45 MeV, but its spectral width is too wide (92.6 keV/ 1σ), which seems to include not only a thermal but also a nonthermal component, such that we could not extract the thermal component, by using the same method as in figure 9.

4.3. Hot electrons for the transverse mode

Figure 13(a) shows that the runaway electron current is the strongest along 21° . Figure 13(b) shows that although the number of electrons both along 21° and 70° is the same as that for the axial mode (figure 13(a)), the number toward 0° is significantly reduced, i.e., the slope temperature is reduced to 1.4 MeV, indicating that the core has significantly absorbed the incoming electrons. Plasmas of $\rho R = 0.011$ g cm $^{-2}$ can absorb electrons having an energy of ≤ 0.075 MeV. Assuming 75% of LFEX was converted to the hot electrons, the absorbed energy would be $0.075/1.4 \times 794 \times 0.75 = 36$ J. Hence, the hot electrons exhibited a η_{electron} value of $36/794 = 4.5\%$ at 75% conversion and 1.8% at 30% conversion at high power.

At LFEX of 342 J (#25T2), the slope temperature was 0.86 MeV, leading to the energy of the absorbed electrons being $0.075/0.86 \times 342 \times 0.75 = 22$ J \pm 3 J at 75% conversion. Thereafter, η_{electron} would be 6.5% at 75% conversion and 2.6% at 30% conversion at the low power.

5. Runaway ions

The energetic ions might have been directly driven by LFEX or secondarily by the LFEX-driven electrons to the core. The ions consisted mainly of deuteron and carbon. ESM simultaneously detected the runaway ions as well as the electrons. Figure 14(b) shows that the number of runaway ions for the transverse mode is approximately 1.5–2 times the number (figure 14(a)) for the axial mode. The reason why this is not so far clear. Since ESM, set at 87.8 cm far from the

target, is too far to discuss a change of a number or spectrum of energetic ions, we could not obtain any heating evidence from ions. Not a ESM, but a track detector much closer to the target than it was here will be used to estimate ion heating.

6. Uniform implosion mode

We aimed to apply the procedure to the previous uniform implosion experiment in 2005 employing 12 GXII beams and PWL to implode and heat, respectively [8]. The ultraintense laser-plasma interaction of this mode must be the same as that of the axial mode in section 3. PWL was another ultraintense laser with a pulse of 190 J \pm 40 J in 0.6 ps. Since the core density was not measured, we presumed the core internal energy to be 50 ± 10 J from the STAR-1D simulation.

Since a uniform implosion must make a core of the same density as or denser than that for the axial mode when the laser energy is the same, the simulated 50 J \pm 10 J [8] would be reasonable compared with 63 J \pm 25 J or 65 J \pm 39 J for the axial or transverse modes, respectively.

The paper revealed that Y_n without PWL heating was $(1.0 \pm 0.6) \times 10^6/4\pi$ sr at a GXII of 1.8 kJ, yielding T_0 of 700 eV \pm 100 eV. PWL of 190 J \pm 40 J enhanced the core x-ray emission to 4.7 ± 0.2 times the emission without PWL, thereby achieving a temperature increment ΔT of $(0.47 \pm 0.01) T_0 = 330 \pm 52$ eV. The core energy increment was $\Delta E = 23$ J \pm 0.5 J, achieving $\eta_{x\text{-ray}}$ of $12\% \pm 2.8\%$.

The thermal neutron was enhanced to $(4.1 \pm 1.2) \times 10^6/4\pi$ sr, that is by (4.1 ± 3.6) times, achieving $\Delta T = (0.26 \pm 0.19) T_0 = 180$ eV \pm 150 eV, $\Delta E = 13$ J \pm 12 J, and $\eta_{\text{neutron}} = 6.8\% \pm 6\%$. The paper also says that the hot electrons transported approximately 15 J from the PWL to the core, which is consistent with the above-discussed ΔE of 23 J–13 J.

Table 1. η obtained from the x-ray, neutrons and hot electrons.

Laser configuration mode (shot #) ^a LFEX power	GXII (J)	LFEX (J)	$\eta_{x\text{-ray}}$	η_{neutron}	$\eta_{\text{electron}} \eta_{75\%} - \eta_{30\%}$ ^b
Axial (#24T3) low power	1657	261	$2.1\% \pm 1.8\%$	$(16\% \pm 14\%)^c$	$1.9 \pm 0.2\% - 0.8\%$
Axial (#4T1) high power	1428	779	$0.5\% \pm 0.4\%$	$2.5\% \pm 1.5\%$	$0.9\% - 0.4\%$
Transverse (#25T2) low power	1740	342	$<7\%$	—	$6.5\% - 2.6\%$
Transverse (#3T2) high power	1378	887	$1.5\% \pm 0.9\%$	$7.7\% \pm 5.5\%$	$4.5\% - 1.6\%$
Uniform [8]	1870 ± 360	190 ± 40	$(12\% \pm 2.5\%)$	$(6.8\% \pm 6\%)$	$(\sim 2.5\%)$

^a# is the shot number.

^b $\eta_{75\%}$ or $\eta_{30\%}$ means η in the case that 75% or 30% of LFEX energy is transported without electrons, respectively.

^c(): the value is uncertain.

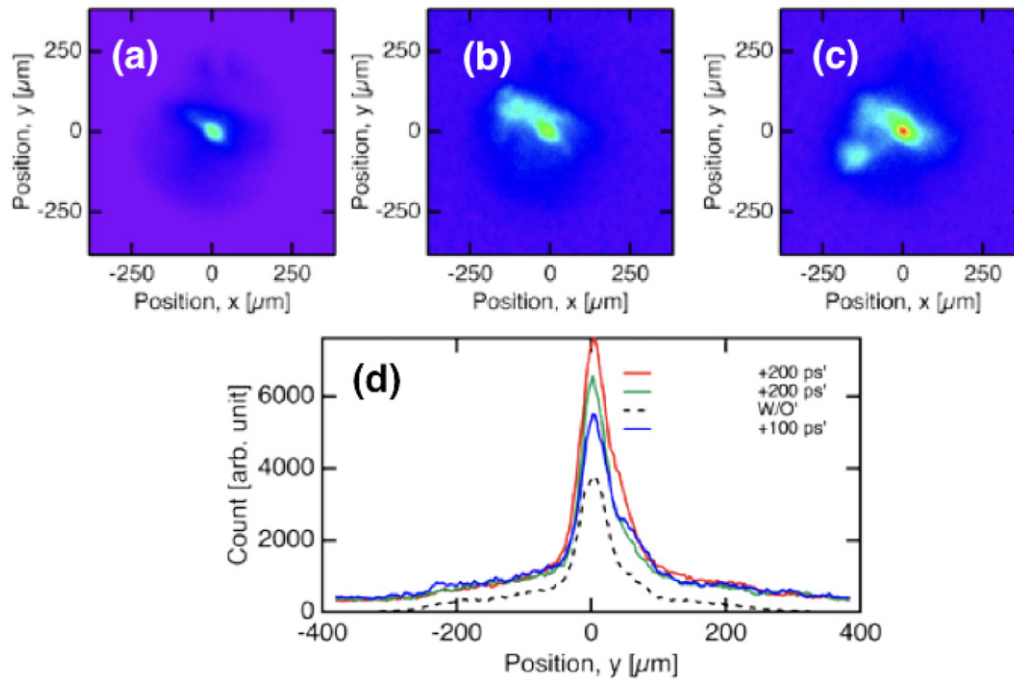


Figure 11. X-ray pinhole images of the core at high power in the transverse mode: (a) without LFEX, and with GXII of 1.33 kJ (#4T3), (b) LFEX of 816 J at +100 ps, and with GXII of 1.44 kJ (#5T4), (c) LFEX of 887 J at +200 ps, and GXII of 1.37 kJ (#3T2); (d) x-axis-scanned emission without LFEX (a) shown by a (a) dashed line (#4T3), (b) blue line (#5T4), and (c) red line (#3T2).

The bremsstrahlung emission due to the hot electron toward 0° was reduced to 70%. Since a 2D PIC simulation predicted a slope temperature of 1.3 MeV, we estimated the deposition to be 4.8 J assuming the same ρR value as the axial mode. Hence, $\eta_{\text{electron}} \sim 2.5\%$.

7. Discussions

Table 1 summarizes the η values that were obtained from the x-ray emissions of the core, the thermal neutrons, and the runaway electrons, respectively. The following points were considered to derive the η : as for the core emission, we assumed that the x-ray emission is close to the blackbody equilibrium state, from the discussion of the mean free path in figure 7(e). However, the core might not be in perfect

equilibrium, except for in the uniform mode (section 6), in which it might be very close to equilibrium.

As for the neutron TOF signals, to derive T_i we preferred Y_n rather than the spectral broadening, because the former is more sensitive than the latter.

To estimate the η from hot electrons, we assumed that almost all of the hot electrons, transported to the core, heat the core.

We did not obtain significant evidence of ion heating. A track detector must be much closer to the target than it was here to estimate ion heating. $\eta_{x\text{-ray}}$, η_{neutron} and η_{electron} for each row in table 1 must agree with a specific value, which will be within the maximum and minimum ones, listed in each row. Hence, for the axial mode we estimate the η within 2.1% and 0.8% at low power, except the values in (), and within 2.5% and 0.4% at high power. For the transverse mode the η will be within

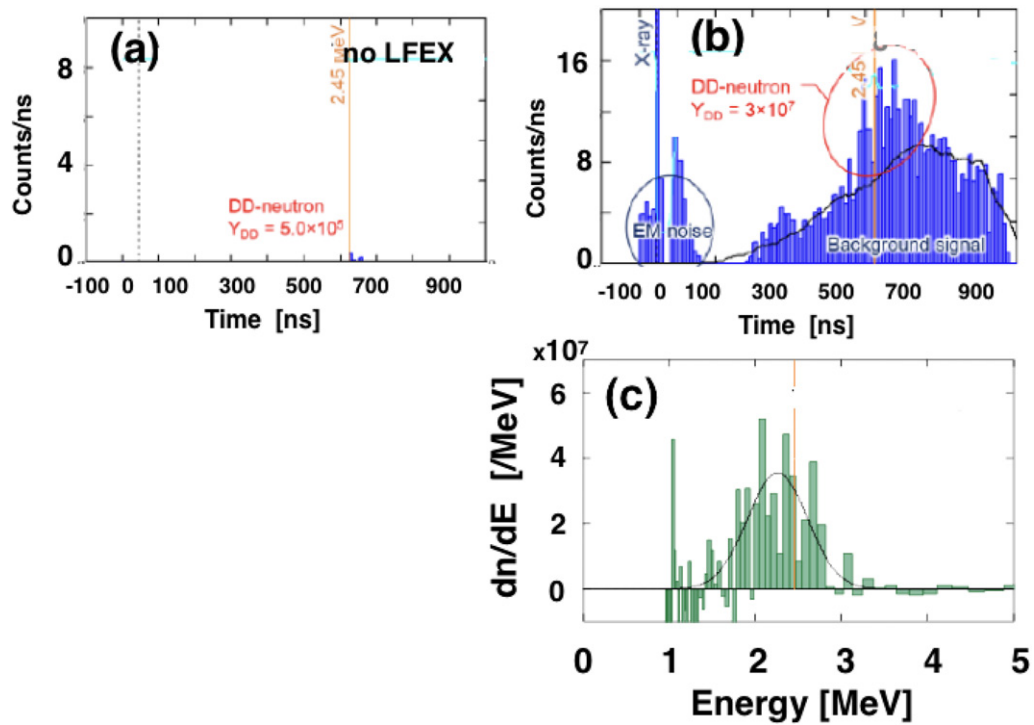


Figure 12. Transverse mode at high power: (a) no LFEX ($\#4T3$), GXII of 1.33 kJ, $Y_n = (5.0 \pm 2.0) \times 10^5/4\pi$ sr, (b) LFEX of 794 J at +200 ps ($\#3T4$), GXII of 1.44 kJ, $Y_n = (3.1 \pm 0.09) \times 10^7/4\pi$ sr. (c) The same as (b) but the background was subtracted.

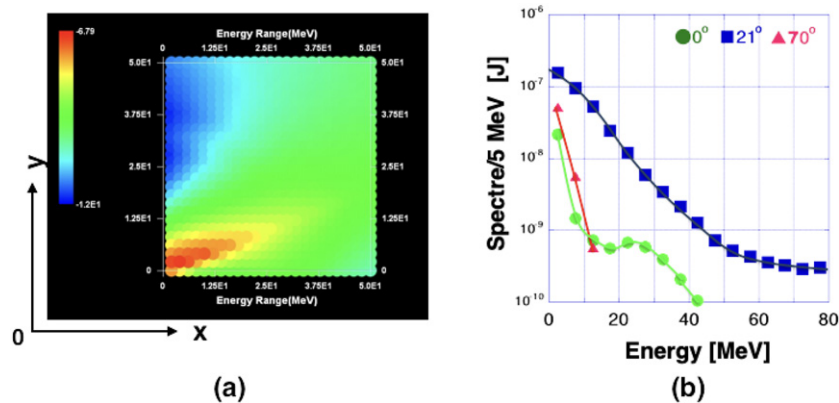


Figure 13. Runaway electron current for the transverse mode at high power ($\#5T4$): (a) spacial current distribution map (red points are along the 21° direction). (b) Current spectrum map: the square is 21° , the solid point is 21° , and the triangle is 70° along the x -axis, LFEX of 794 J at +200 ps (at high power $\#3T4$) and GXII of 1.44 kJ.

7% and 2.6% at low power, and will be within 7.7% and 1.5% at high power. Comparison between the transverse and axial modes shows the η for the transverse mode appears higher than that for the axial mode either at the low or high power. STAR-2D predicted that the core density for the transverse mode is somewhat higher than that for the axial one, which makes the η for the transverse mode higher than that for the axial.

The fact that the hot-electron slope temperature of 8.7 MeV for the axial mode decreased to 1.4 MeV for the transverse mode, shows that LFEX propagates through an underdense plasma around the core for longer distance for the axial mode than for the transverse one. Then for the axial mode the hot

electrons are more dissipated and reduce coupling with the core. This can explain the result that the η for the transverse mode appears higher than that for the axial mode.

For the uniform mode (the last row in table 1), $\eta_{x\text{-ray}}$ is not so far from the η_{neutron} , within a twice, which shows the procedure used here may be able to estimate the η . However, since we have not measured the core density, we cannot definitely estimate the η . It is noted that the x -ray gives higher η than the neutron.

The η for the uniform mode is closer to the transverse mode, although we have thought it would be close to the η for the axial mode. Since LFEX (PWL) in the uniform mode must encounter a similar plasma cloud as in the axial mode, the η

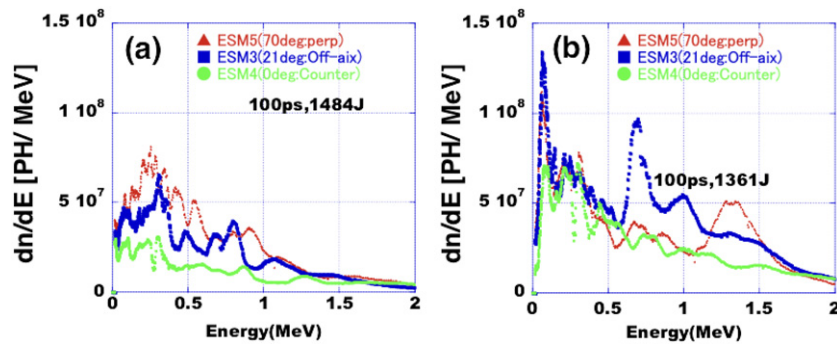


Figure 14. Runaway ion spectrum for (a) the axial mode at high power (#4T2; GXII is 1.34 kJ), and for (b) transverse mode (#5T4; GXII is 1.43 kJ). The green (solid circle) is for 0° , blue (square) is 21° , and red (triangle) is 70° along the x -axis.

is supposed to be as same as in the axial mode. The present experimental results, however, seem to show that the η in the uniform mode is closer to the transverse mode. This will be because the uniform implosion provides a denser core, which makes LFEX couple with the core. Although the energy of LFEX is small in the uniform mode, the η was close to the present transverse mode, which leads us to believe that increasing the core ρR will give higher η for both axial and transverse modes in the future.

Although we expect that $\eta_{x\text{-ray}}$ and η_{neutron} are close to each other, table 1 shows η_{neutron} is around 5 times as much as $\eta_{x\text{-ray}}$ both for the axial and transverse modes. Since the neutron yield varies statistically from a twice to a half when the yield into the detector is a few, the x-ray emission may be more reliable than the neutron yield. Another reason why may be that the core emission is not in perfect equilibrium.

There is an another possible emission, which is the bremsstrahlung emission from a thermal plasma, given by $1.53 \times 10^{-32} Z^2 T^{1/2} (\text{eV}) N_+ N_e (\text{J cm}^{-3} \text{s}^{-1})$. In this case, T is not proportional to the one fourth power of x-ray emission. The exponent is not $1/4$, but is between $1/4$ for the Planck and 2 for the bremsstrahlung, which will increase $\eta_{x\text{-ray}}$ so close to η_{neutron} . Since the bremsstrahlung emission is proportional to $T^{1/2}$, the emission ratio of 2 for the axial mode, for instance, provides a temperature enhancement of 3, or $\Delta T = 1.5 \text{ keV}$. But it provides too high neutron yield than the experimental value. The emission ratio of 4.7 for the uniform mode provides a temperature enhancement of 22, or ΔT of unrealistic 15 keV. Hence, we think the detected emission is not due to the bremsstrahlung.

In another study [10, 11], only two beams from GXII had imploded a similar CD shell, to which LFEX was illuminated. The energies of GXII and LFEX were 254 J and 613 J, respectively. The neutron yield was enhanced by 100 fold, from which we estimated $\eta_{\text{neutron}} = 3.5\% \pm 3\%$, assuming $\rho = 2 \text{ g cm}^{-3}$. The laser configuration was similar to the present transverse mode and the current result is comparable. However, the error bar was too large to confirm that this true.

Using a GXII-precompressed solid ball with a cone and LFEX of 625 J, Sakata *et al*, had reported that the maximum laser-to-core coupling efficiency by drag heating is $7.7\% \pm 1.2\%$ [25, 26]. The core density, ρ , was simulated to be 11.3 g cm^{-3} .

8. Conclusion

The efficiency η of the fast heating was investigated, when a pre-imploded core was directly illuminated by an ultraintense laser. The η is defined as an increase of the internal core energy divided by the heating laser energy. Six beams (output 1.6 kJ) from the GXII green laser system at the ILE, Osaka University were applied to implode a spherical CD (deuterated polystyrene) shell target to form a dense core.

For the pre-imploded core:

- The DD-reacted protons and the x-ray emission observed for the axial mode resulted in a core volume of $(3.2 \pm 0.5) \times 10^{-7} \text{ cm}^3$ and density of $(2.87 \pm 0.7) \text{ g cm}^{-3}$, or 2.6 times the solid density.
- For the transverse mode, the core volume was $(4.4 \pm 0.7) \times 10^{-7} \text{ cm}^3$. The density was not measured, but STAR-2D predicted that it is the same or somewhat larger than that of the axial mode.
- The DD-reacted thermal neutrons resulted in core temperatures of $0.75 \text{ keV} \pm 0.1 \text{ keV}$ and $0.6 \text{ keV} \pm 0.05 \text{ keV}$ for axial and transverse modes, respectively.

As for LFEX heating, we have found the η from three independent methods: (1) the core x-ray emission, (2) the thermal neutron yield, and (3) the runaway hot electron spectra. The results were as follows:

- For the axial mode, $0.8\% < \eta < 2.1\%$ at the low power (low LFEX energy) and $0.4\% < \eta < 2.5\%$ at high power (high LFEX energy).
- For the transverse mode, $2.6\% < \eta < 7\%$ at the low power and $1.5\% < \eta < 7.7\%$ at high power.
- Comparison between the articles (a) and (b) shows the η for the transverse mode appears higher than that for the axial mode either at the low or high power.
- The η for the uniform mode, $6\% < \eta < 12\%$ appears near that of the transverse mode, although the error bar for the uniform mode is very large. We have obtained values of η in the nonuniform implosions close to that in the uniform implosion.

As a first step of the fast ignition study, we have a value of η to be around 5%. The uniform mode makes us expect that

increasing the core ρR will give higher η for both axial and transverse modes in the future. The ion heating of the core is a future challenge.

Acknowledgments

The authors wish to acknowledge the LFEX and GXII operation, measurement, and target fabrication teams at the ILE, Osaka University. This work is performed under the collaborative research program of ILE (2018B2-KITAGAWA) and with the support and under the auspices of the NIFS Collaborative Research Program (NIFS18KUGK124: 2018FO-03, 2019FP-03). The authors would like to thank Enago (www.enago.jp) for the English language review.

ORCID iDs

Yoshitaka Mori  <https://orcid.org/0000-0001-7754-9171>
 Atsushi Sunahra  <https://orcid.org/0000-0001-7543-5226>
 Tomoyuki Johzaki  <https://orcid.org/0000-0002-5738-4661>
 Shinsuke Fujiokua  <https://orcid.org/0000-0001-8406-1772>
 Akifumi Yogo  <https://orcid.org/0000-0003-3412-0070>

References

- [1] Lindl J.D. 1998 *Inertial Confinement Fusion: The Quest for Ignition and Energy Gain Using Indirect Drive* (New York: Springer)
- [2] Hurricane O.A. et al 2014 *Nature* **506** 343–8
- [3] Le Pape S. et al 2018 *Phys. Rev. Lett.* **120** 245003
- [4] Tabak M., Hammer J., Glinsky M.E., Kruer W.L., Wilks S.C., Woodworth J., Campbell E.M., Perry M.D. and Mason R.J. 1994 *Phys. Plasmas* **1** 1626
- [5] Brueckner K.A. and Jorna S. 1974 Laser-driven fusion *Rev. Mod. Phys.* **46** 325–67
- [6] Kitagawa Y. et al 2001 *43rd APS DPP Meeting* vol QI2.006 (Long Beach, CA, 29 October–2 November 2004)
- [7] Kitagawa Y. et al 2004 *IEEE J. Quantum Electron.* **40** 281
- [8] Kitagawa Y. et al 2005 *Phys. Rev. E* **71** 016403
- [9] Kitagawa Y. et al 2005 *J. Plasma Fusion Res.* **81** 384
- [10] Kitagawa Y. et al 2015 *Phys. Rev. Lett.* **114** 195002
- [11] Kitagawa Y. et al 2017 *Nucl. Fusion* **57** 076030
- [12] Miura E. et al 2020 *High Energy Density Phys.* **37** 100890
- [13] Kitagawa Y. et al 1995 *Phys. Rev. Lett.* **75** 3131–3
- [14] Arikawa Y. et al 2012 *Rev. Sci. Instrum.* **83** 10D909
- [15] Abe Y. et al 2020 *High Energy Density Phys.* **36** 100803
- [16] Abe Y. et al (GEKKO-XII and LFEX Team) 2014 *Plasma Fusion Res.* **9** 4404110
- [17] Zel'dovich Y.B. and Raizer Y.P. 1976 *Physics of Shock Waves and High-Temperature Hydrodynamic Phenomena* vol 1 (New York: Academic) p 116
- [18] Atzeni S. and Meyer-ter-Vehn J. 2004 *The Physics of Inertial Fusion* (Oxford: Clarendon) p 360
- [19] Knoll G.F. 1989 *Radiation Detection and Measurement* 2nd edn (New York: Wiley) ch 2
- [20] Tajima T. and Dawson J.M. 1979 *Phys. Rev. Lett.* **43** 267
- [21] Kitagawa Y. et al 1992 *Phys. Rev. Lett.* **68** 48
- [22] Ozaki T. et al 2015 *J. Phys.: Conf. Ser.* **717** 012043
- [23] Freeman R.R., Batani D., Baton S., Key M. and Stephens R. 2006 *Fusion Sci. Technol.* **49** 297
- [24] Norreys P. et al 2014 *Nucl. Fusion* **54** 054004
- [25] Sakata S. et al 2018 *Nat. Commun.* **9** 3937
- [26] Matsuo K. et al 2020 *Phys. Rev. Lett.* **124** 035001